Appl. Phys. A (2016) 122:1036
DOI 10.1007/s00339-016-0576-8

Applied Physics A
Materials Science & Processing

Deep ultraviolet photodetectors based on *p*-Si/*i*-SiC/*n*-Ga_2O_3 heterojunction by inserting thin SiC barrier layer

Yuehua An[1,2] · Yusong Zhi[1,2] · Zhenping Wu[1,2] · Wei Cui[1,2] · Xiaolong Zhao[1,2] · Daoyou Guo[2] · Peigang Li[1,2] · Weihua Tang[1,2]

Received: 21 June 2016 / Accepted: 17 November 2016 / Published online: 21 November 2016

Abstract Deep ultraviolet photodetectors based on *p*-Si/*n*-Ga_2O_3 and *p*-Si/*i*-SiC/*n*-Ga_2O_3 heterojunctions were fabricated by laser molecular beam epitaxial (L-MBE), respectively. In compare with *p*-Si/*n*-Ga_2O_3 heterostructure-based photodetector, the dark current of *p*-Si/*i*-SiC/*n*-Ga_2O_3-based photodetector decreased by three orders of magnitude, and the rectifying behavior was tuned from reverse to forward. In order to improve the quality of the photodetector, we reduced the oxygen vacancies of *p*-Si/*i*-SiC/*n*-Ga_2O_3 heterostructures by changing the oxygen pressure during annealing. As a result, the rectification ratio (I_F/I_R) of the fabricated photodetectors was 36 at 4.5 V and the photosensitivity was 5.4×10^5% under the 254 nm light illumination at −4.5 V. The energy band structure of *p*-Si/*n*-Ga_2O_3 and *p*-Si/*i*-SiC/*n*-Ga_2O_3 heterostructures was schematic drawn to explain the physic mechanism of enhancement of the performance of *p*-Si/*i*-SiC/*n*-Ga_2O_3 heterostructure-based deep UV photodetector by introduction of SiC layer.

✉ Peigang Li
pgli@zstu.edu.cn

✉ Weihua Tang
whtang@bupt.edu.cn

[1] Laboratory of Optoelectronics Materials and Detectors, School of Science, Beijing University of Posts and Telecommunications, Beijing 100876, China

[2] State Key Laboratory of Information Photonics and Optical Communications, Beijing University of Posts and Telecommunications, Beijing 100876, China

1 Introduction

β-Ga_2O_3-based ultraviolet (UV) photodetectors [1–7], such as *p*–*n* junctions, metal–semiconductor–metal (MSM) and Schottky barrier structures, have attracted intensitive attentions due to the unique physical properties of *β*-Ga_2O_3, including a direct band gap of 4.9 eV, high transparency, low cost and high resistance to radiation. Compared with MSM photodetector, junction-based detector usually exhibits extraordinary behavior, such as large photoelectric responsivity and fast response speed. On the other hand, *β*-Ga_2O_3 shows a n-type semiconductor due to the presence of a donor band related to intrinsic oxygen deficiency [8, 9]. Thus, a p-Si/n-Ga_2O_3 heterojunction photodetector has been developed owing to the low cost of the Si substrate and easy fabricated for integrated circuits [7]. However, a large dark current is critical issues associated with the heterojunction photodetectors owing to the thick Si substrate [7, 10]. In fact, the dark current can be reduced by inserting an intrinsic (*i*) layer between p and n layers [11–14]. Recently, Chen et al. reported that the *n*-ZnO/*p*-Si NWs photodiodes exhibit high responsivity under a reverse bias by inserting an ultrathin SiO_2 layer on top of Si NWs [15]. Alternatively, Guo et al. reported that *n*-ZnO/*i*-MgO/*p*-Si photodetector showed a rectification ratio of about 10^4 at 2 V and a dark current of 0.5 nA at −2 V [16]. Based on the literatures mentioned above, SiC as a wide band gap material is promised to be an appropriate hole blocking layer to improve photoelectric performances of *p*-Si/*i*-SiC/*n*-Ga_2O_3 photodetectors.

In this study, *p*-Si/*n*-Ga_2O_3 and *p*-Si/*i*-SiC/*n*-Ga_2O_3 UV photodetectors were fabricated by different oxygen pressure. The UV photodetectors exhibit advantageous photoelectric performances by introducing SiC layer and

modulating oxygen vacancy, such as the increase in rectifying ratio and the enhancement of photoresponse property.

2 Experimental

The *p*-Si/*n*-Ga_2O_3 and *p*-Si/*i*-SiC/*n*-Ga_2O_3 heterojunction photodetectors were fabricated using L-MBE technique. The laser ablation with a fluence of 5 J/cm^2 was carried out with a repetition rate of 1 Hz by using a KrF excimer laser with a wavelength of 248 nm. The distance between target and substrate was 5 cm, and the substrate was rotated during deposition to improve the film uniformity. Two targets of pure Ga_2O_3 and pure SiC were employed to deposit Ga_2O_3 and *i* layer SiC thin films, respectively. The base pressure in chamber was 1×10^{-6} Pa. The substrate temperature was kept at 750 °C. For *p*-Si/*i*-SiC/*n*-Ga_2O_3 deposition in vacuum (p–i–n D in V), SiC film was deposited for 4000 pulse before the Ga_2O_3 film was deposited for 7000 pulse upon vacuum conditions, then annealing for 1 h under 1 Pa oxygen pressure. For *p*-Si/*i*-SiC/*n*-Ga_2O_3 deposition in O_2 (p–i–n D in O_2), SiC film was deposited for 4000 pulse upon vacuum conditions, and then, the Ga_2O_3 film was deposited for 7000 pulse under 1×10^{-3} Pa oxygen pressure, followed annealing for 1 h under 1 Pa oxygen pressure. And in order to avoid SiC layer oxidized, Ga_2O_3 film deposited 5 min upon vacuum conditions before under 1×10^{-3} Pa oxygen pressure. The thickness of the SiC films and Ga_2O_3 films were estimated by scanning electron microscope (SEM) to be about 70 and 400 nm, respectively. The crystal structure was measured by a Bruker D8 Advance X-ray diffractometer (XRD). The surface of thin film was checked in situ by means of reflection high-energy electron diffraction (RHEED). The oxygen vacancies of as-grown and post-annealing samples were investigated by X-ray photoelectron spectroscopy (XPS). Au/Ti (100 nm) and Au (100 nm) electrodes (radius = 1 mm) were successively sputtered as cathode for n-Ga_2O_3 thin film and anode p-type silicon substrate, a good ohmic contacts were achieved in both electrodes for all the detectors. The I–V curves and time-dependent photoresponse of the photodetectors were measured by Keithley 2450. A 6 W lamp was employed to provide the 254 nm UV for the photocurrent measurement.

3 Result and discussion

Figure 1 shows the XRD patterns of three samples. The peaks located at around 18.94°, 38.42° and 59.08° are observed, corresponding to β-Ga_2O_3 $(\bar{2}01)$, $(\bar{4}02)$ and $(\bar{6}03)$ orientations. The result indicates that the β-Ga_2O_3 is deposited with single orientation along the $(\bar{2}01)$ direction.

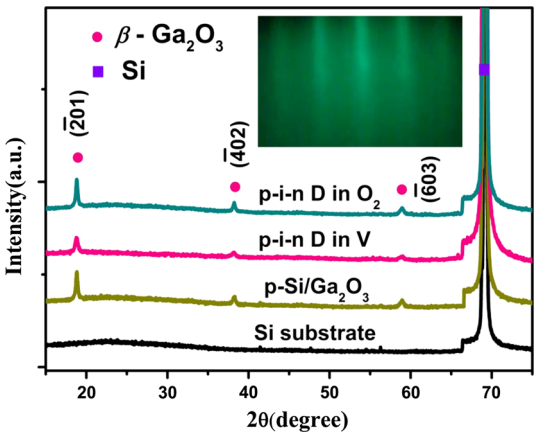

Fig. 1 XRD pattern of the β-Ga_2O_3 thin films and Si substrate. *Inset* shows RHEED image of *p*-Si/*i*-SiC/*n*-Ga_2O_3 deposition in O_2

No characteristic peak of SiC was observed, which reveals that the SiC thin film is amorphous. The inset image shows the RHEED pattern of *p*-Si/*i*-SiC/*n*-Ga_2O_3 deposition in O_2. Conspicuous streak patterns imply that the Ga_2O_3 film has a good crystallized structure with smooth surface. The intensity of the diffraction peaks of *p*-Si/*i*-SiC/*n*-Ga_2O_3 deposition in O_2 is higher to *p*-Si/*i*-SiC/*n*-Ga_2O_3 deposition in vacuum. It means that defect of the β-Ga_2O_3 thin film was reduced by decreasing oxygen pressure. However, oxygen pressure has not influenced the lattice parameters of films, for no shift of the β-Ga_2O_3 diffraction peaks position is observed in these samples. The growth condition of Ga_2O_3 thin film of *p*-Si/*n*-Ga_2O_3 is same with that of *p*-Si/*i*-SiC/*n*-Ga_2O_3 deposition in O_2, and the *p*-Si/*n*-Ga_2O_3 photodetector was studied in our group in detail [7]. So, we mainly focused on the investigation of the samples with SiC layer in this study.

Figure 2 shows the O1 s peak of *p*-Si/*i*-SiC/*n*-Ga_2O_3 deposition in vacuum and *p*-Si/*i*-SiC/*n*-Ga_2O_3 deposition in O_2, which can be divided into two components (I and II). The II peak that is usually associated with oxygen vacancy

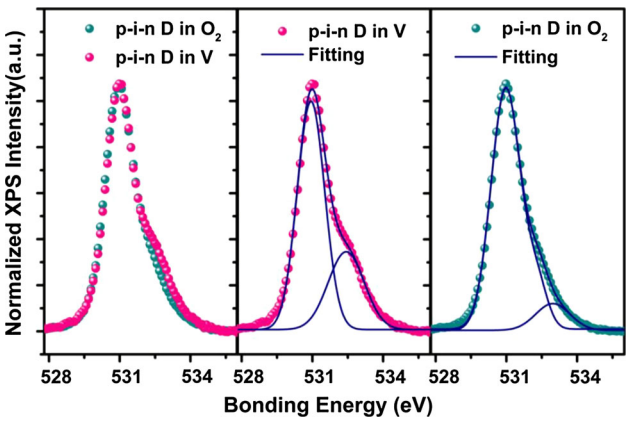

Fig. 2 Normalized O 1 s XPS spectra of *p*-Si/*i*-SiC/*n*-Ga_2O_3 heterojunction photodetectors

[6] is highly suppressed with higher oxygen pressure during film deposition, indicating that the oxygen vacancy concentration decreased. Thus, it is reasonable to infer that oxygen vacancy concentration in the β-Ga_2O_3 thin films can be tuned by using different oxygen pressure.

Figure 3b shows the I–V characteristics of p-Si/i-SiC/n-Ga_2O_3 deposition in vacuum and p-Si/i-SiC/n-Ga_2O_3 deposition in O_2 under dark condition, in which the I–V curve of p-Si/n-Ga_2O_3 structure is also presented for comparison. The schematic drawing of fabricated prototype heterojunction UV photodetector is shown in Fig. 3a. The ohmic contact of Au/Ti/n-Ga_2O_3/SiC on a sapphire substrate and Au/Ti/SiC has been confirmed by the linear I–V curve under the same conditions (inset in Fig. 3b). The resistance of SiC is greater than that of Ga_2O_3. So, SiC layer plays the role of an appropriate electron-blocking layer in this work. A reverse rectifying behavior is observed in the conventional p-Si/n-Ga_2O_3 photodetector [7]. However, I–V characteristics of p-Si/i-SiC/n-Ga_2O_3 deposition in vacuum and p-Si/i-SiC/n-Ga_2O_3 deposition in O_2 exhibit forward rectifying behavior by inserting i-SiC layer. Meanwhile, compared with the p-Si/n-Ga_2O_3 photodetector, the dark current of p–i–n structure (p-Si/i-SiC/n-Ga_2O_3 deposition in O_2) is effectively reduced by three orders of magnitude owing to the insertion of i-SiC layer. Additionally, p-Si/i-SiC/n-Ga_2O_3 deposition in O_2 shows a lower dark current than that of p-Si/i-SiC/n-Ga_2O_3 deposition in vacuum due to oxygen vacancy decrease.

In order to further check the solar blind UV responsivity of the photodetector, we measure the I–V curves of p-Si/i-SiC/n-Ga_2O_3 deposition in vacuum and p-Si/i-SiC/n-Ga_2O_3 deposition in O_2 in dark and under the 254 nm light illumination, respectively. The power density of 254 nm light is 12 μW/cm^2. Figure 4a shows the I–V curves of photodetectors with log-linear scale. Compared with corresponding dark currents, the photocurrents of p-Si/i-SiC/n-Ga_2O_3 deposition in O_2 and p-Si/i-SiC/n-Ga_2O_3 deposition in vacuum increase from 3.2×10^{-8} A and 2.2×10^{-6} A to 1.9×10^{-4} A and 7.4×10^{-4} A under the 254 nm light illumination at −4.5 V. The photosensitivity is defined as $(I_{light}–I_{dark})/I_{dark}$ as a percentage (I_{light} is the current of the detector when illuminated with a light, and I_{dark} is the dark current). Under the 254 nm light illumination with a bias voltage of −4.5 V, the photosensitivity of the p-Si/i-SiC/n-Ga_2O_3 deposition in O_2 is found to be 5.4×10^5%, which is much higher than that of p-Si/i-SiC/n-Ga_2O_3 deposition in vacuum (3.4×10^4%).

In Fig. 4b, the log–log scale plot of the injection currents for p-Si/i-SiC/n-Ga_2O_3 deposition in vacuum and p-Si/i-SiC/n-Ga_2O_3 deposition in O_2 shows three different regions depending on the range of the junction voltage. In a very low voltage for $V < -0.28$ V (region I), the detectors show high resistance and a linear dependence of the current on the voltage (I–V) is observed, indicating that the transport mechanism obeys ohmic law. In region II, $-0.28\ V < V < -1$ V, the currents increased exponentially following a relation $I \sim exp(\alpha V)$, which is usually observed in the wide band gap (p–n) detector due to a recombination tunneling mechanism [10]. By fitting the experimental data, the constant α of p-Si/i-SiC/n-Ga_2O_3 deposition in vacuum and p-Si/i-SiC/n-Ga_2O_3 deposition in O_2 has been evaluated to be 0.6 and 0.57 V^{-1} (falling in the range of 0.45–1.45 V^{-1} for the semiconductor junctions), which explains the high carrier (electrons) injection. However, beyond −1 V, the current across the junction is dominated by the holes injection because the concentration and mobility of the holes in Si are higher than those of electrons in Ga_2O_3.

Before explaining the transport mechanism, it is necessary to understand the energy band diagram of the junction.

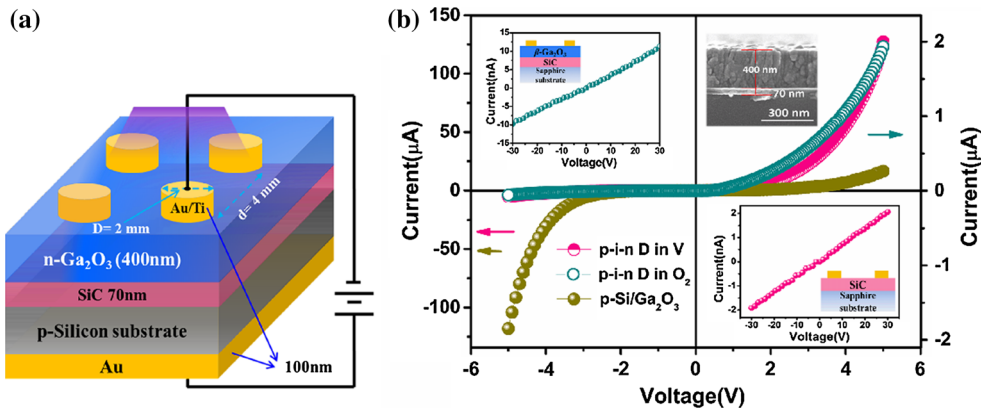

Fig. 3 **a** Schematic diagram of p-Si/i-SiC/n-Ga_2O_3 heterojunction photodetector; **b** I–V curves of p-Si/i-SiC/n-Ga_2O_3 heterojunctions photodetectors in *dark* that of conventional p-Si/n-Ga_2O_3 heterojunction detector is also presented for comparison. The *insets*, respectively, show I–V characteristics of the n-Ga_2O_3/SiC heterojunction (*top left*) and the SiC layer (*bottom right*) prepared on a sapphire substrate under vacuum condition

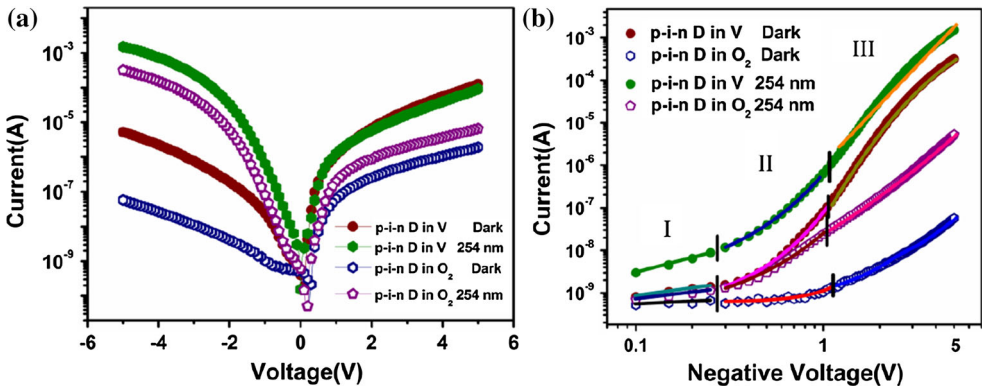

Fig. 4 **a** Responsivity of *p*-Si/*i*-SiC/*n*-Ga_2O_3 heterojunction photodetectors at different bias in *dark* and under the 254 nm light illumination. **b** Log–log plots of the injection current versus voltage in negative bias

Figure 5a shows the band diagram of the *p*-Si/*i*-SiC/*n*-Ga_2O_3 photodetector. The electron affinity of χ_{Ga2O3}, χ_{SiC} and $\chi_{p\text{-}Si}$ was 4.0, 3.45 and 4.05 eV, respectively. The band gap of Ga_2O_3, SiC and *p*-Si was 4.9, 3.2, and 1.12 eV. According to the Anderson model, the conduction band offset of Ga_2O_3/SiC was $\Delta E_c = 0.55$ eV, and the valence band offset of SiC/*p*-Si was $\Delta E_v = 1.48$ eV.

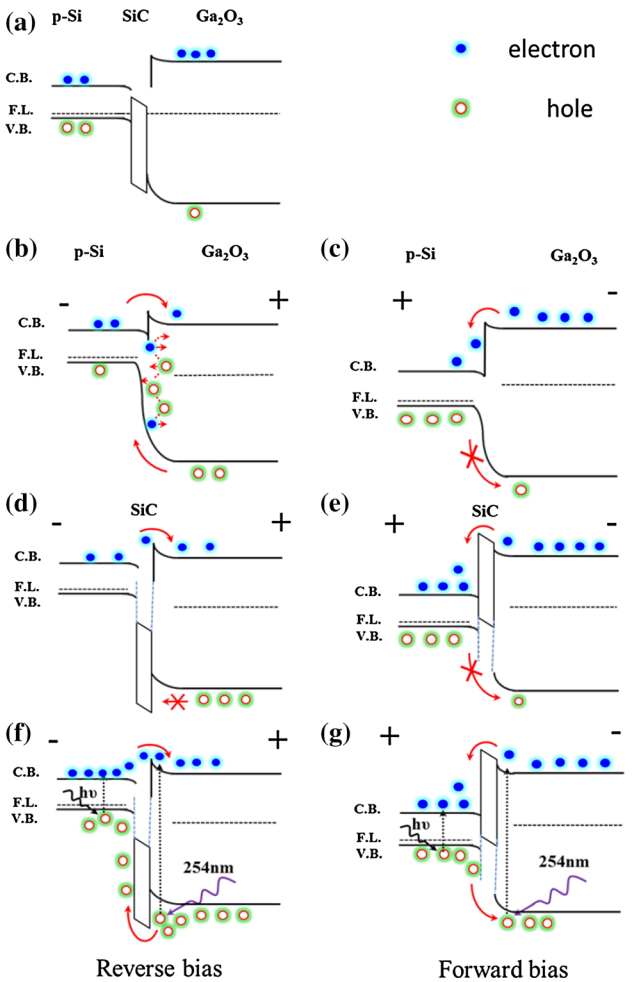

Fig. 5 Energy band diagrams for detectors based on *p*-Si/*i*-SiC/*n*-Ga_2O_3 heterojunction **a** no biased and biased in the **b**, **d**, **f** forward and **c**, **e**, **g** reverse directions at 4.5 V

Without the insulated layer, electrons will drift from *p*-Si to Ga_2O_3, while holes drift from Ga_2O_3 to *p*-Si under reverse bias. In contrast, most of the electrons and holes in depletion receive high energy from the strong electric filed in barrier region and collide with lattice atoms of barrier region. The electrons of valence are collided, creating conduction electron and valence hole. Thus, avalanche effect appeared in the depletion layer and produces a large number of carriers. It leads to the enhancement of reverse current [7].

The situations are different with the presence of the SiC appropriate electron-blocking layer. Under the reverse bias, most of the voltage will be applied on the SiC layer due to its dielectric nature. Thus, the bands of SiC will be bended, and the effective barrier in the vicinity of valence band is greatly increased. Consequently, electrons in the *p*-Si layer can cross the barrier and enter into the Ga_2O_3 layer, while holes will be confined in the Ga_2O_3 layer by large valence band offset between Ga_2O_3 and SiC due to the SiC dielectric layer (Fig. 5d). Under the positive voltage, the band offsets of Ga_2O_3/SiC was 0.55 eV, and the electrons in *n*-Ga_2O_3 were considerably larger than that of the *p*-Si, the plenty of electrons in the Ga_2O_3 layer absorbing energy though the SiC barrier enter into *p*-Si layer (Fig. 5e). Ultimately, the current under the positive bias is greater than the one under the reverse bias.

When the detector at a reverse bias is illuminated by 254 nm light, the light is absorbed in the depletion region near *i*-SiC/*n*-Ga_2O_3 interface; the photo-generated carriers are extracted to the outer circuit. The photo-generated holes cross the barrier into the *p*-Si. On the other hand, our Ga_2O_3 film is highly transparent above 250 nm, meaning that electrons–hole pairs are produced in the *p*-Si layer when it absorbs UV photons. The photo-generated electronics cross the barrier into the Ga_2O_3 layer. Therefore, the photocurrents greatly increase (Fig. 5f). Under the positive voltage, the photo-generated electronics cross the barrier into the *p*-Si layer. Therefore, parts of light cross the

Ga_2O_3 layer into the p-Si, electronics and holes produced in the p-Si. These photo-generated electronics cross the SiC barrier into the Ga_2O_3 (Fig. 5g).

4 Conclusion

The p-Si/i-SiC/n-Ga_2O_3 heterojunction-based photodetectors were fabricated by inserting SiC appropriate electron-blocking layer between Ga_2O_3 film and p-Si substrate. The oxygen vacancies were reduced by changing the annealing process. After introduction of SiC layer and reduction in oxygen vacancies, the performance of the photodetector was obviously improved. The experimental results reported here demonstrated a potential application of p-Si/i-SiC/n-Ga_2O_3 heterojunction in photoelectronic devices. And the process described here might be also helpful for design and fabrication photoelectronic devices based on Ga_2O_3.

Acknowledgements This work was supported by the National Natural Science Foundation of China (Grant Nos. 51572033, 61274017, 51572241 and 11404029).

References

1. L. Li, E. Auer, M. Liao, X. Fang, T. Zhai, U.K. Gautam, A. Lugstein, Y. Koide, Y. Bando, D. Golberg, Nanoscale **3**, 1120–1126 (2011)
2. Y.H. An, D.Y. Guo, S.Y. Li, Z.P. Wu, Y.Q. Huang, P.G. Li, L.H. Li, W.H. Tang, J. Phys. D Appl. Phys. **49**, 285111 (2016)
3. Y.H. An, D.Y. Guo, Z.M. Li, Z.P. Wu, Y.S. Zhi, W. Cui, X.L. Zhao, P.G. Li, W.H. Tang, RSC Adv. **6**, 66924 (2016)
4. R. Suzuki, S. Nakagomi, Y. Kokubun, N. Arai, S. Ohira, Appl. Phys. Lett. **94**, 222102 (2009)
5. Y.H. An, X.L. Chu, Y.Q. Huang, Y.S. Zhi, D.Y. Guo, P.G. Li, Z.P. Wu, W.H. Tang, Prog. Nat. Sci: Mater. **26**, 65–68 (2016)
6. D.Y. Guo, Z.P. Wu, Y.H. An, X.C. Guo, X.L. Chu, C.L. Sun, L.H. Li, P.G. Li, W.H. Tang, Appl. Phys. Lett. **105**, 023507 (2014)
7. X.C. Guo, N.H. Hao, D.Y. Guo, Z.P. Wu, Y.H. An, X.L. Chu, L.H. Li, P.G. Li, M. Lei, W.H. Tang, J. Alloy. Compd. **660**, 136–140 (2016)
8. J. Varley, J. Weber, A. Janotti, C. Van de Walle, Appl. Phys. Lett. **97**, 142106 (2010)
9. Y.H. An, Y.S. Zhi, W. Cui, X.L. Zhao, Z.P. Wu, D.Y. Guo, P.G. Li, W.H. Tang, J. Nanosci. Nanotechnol. **17**, 1–4 (2017)
10. M.L. Lee, P.F. Chi, J.K. Sheu, Appl. Phys. Lett. **94**, 013512 (2009)
11. H. Zhu, C.X. Shan, B. Yao, B.H. Li, J.Y. Zhang, Z.Z. Zhang, D.X. Zhao, D.Z. Shen, X.W. Fan, Y.M. Lu, Z.K. Tang, Adv. Mater. **21**, 1613–1617 (2009)
12. J.C. Carrano, T. Li, P.A. Grudowski, C.J. Eiting, D. Lambert, J.D. Schaub, R.D. Dupuis, J.C. Campbell, Electron. Lett. **34**, 692–693 (1998)
13. Y. Irokawa, B. Luo, J. Kim, J.R. LaRoche, F. Ren, K.H. Baik, S.J. Pearton, C.C. Pan, G.T. Chen, J.I. Chyi, S.S. Park, Y.J. Park, Appl. Phys. Lett. **83**, 2271–2273 (2003)
14. J.D. Hwang, D.H. Wu, S.B. Hwang, Photon. Technol. Lett. IEEE **26**, 1081–1084 (2014)
15. C.Y. Huang, Y.J. Yang, J.Y. Chen, C.H. Wang, Y.F. Chen, L.S. Hong, C.S. Liu, C.Y. Wu, Appl. Phys. Lett. **97**, 013503 (2010)
16. T.C. Zhang, Y. Guo, Z.X. Mei, C.Z. Gu, X.L. Du, Appl. Phys. Lett. **94**, 113508 (2009)